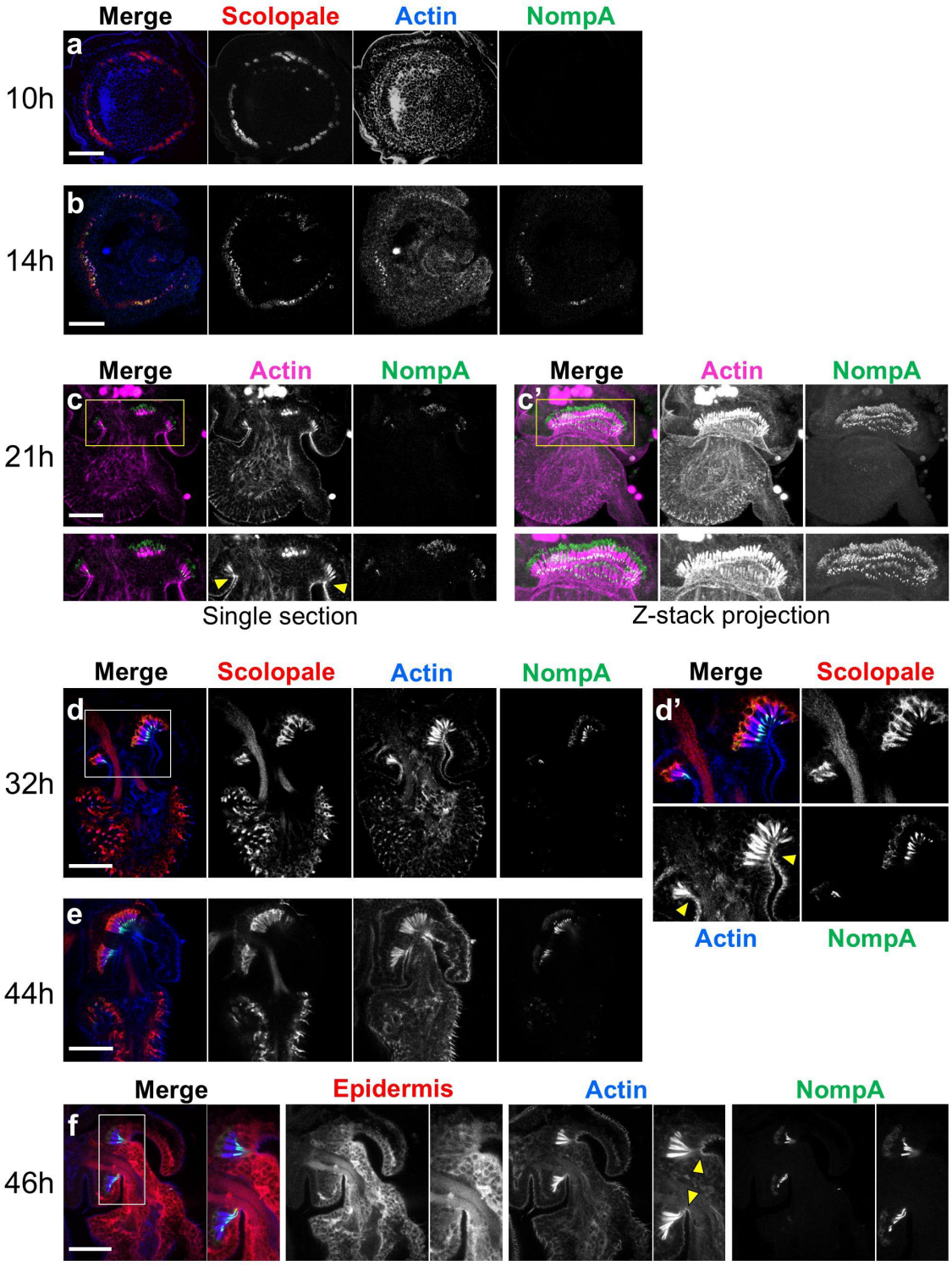


Fig. S1 Expression of scolopidium markers in the antenna, related to Fig. 3. Antennae fixed at the indicated hours APF are shown. Scolopale cell membranes, Actin and NompA are visualized as in Fig. 3. **(a)** At 10 hours APF, scolopale cells are labeled by *pros*-GAL4-driven expression of mCD8::RFP, while GFP-NompA is not detected. **(b)** GFP-NompA is detected in some scolopale cells at 14 hours APF. **(c, c')** A single confocal section (c)

and a Z-stack projection (c') of an antenna at 21 hours APF (the same antenna as shown in Fig. 3d), viewed along the anterior-posterior axis. Lower panels are magnified views of the boxed regions in the upper panels. GFP-NompA and actin structures (scolopale rods and cap rods, as shown in Fig. 3d, d') are present in all scolopidia along the entire perimeter of the a2-a3 joint, where the epidermis has invaginated (arrowheads). **(d-f)** Single confocal sections of antennae at indicated hours APF (the same antennae as shown in Fig. 3e-f). (d') is a magnified view of the boxed region in (d). Scolopidia encircle and connect to the deepest point of the epidermal invagination at a2-a3 joint (arrowheads). Images in (c-e) are flipped horizontally. Scale bars: 50 μm.

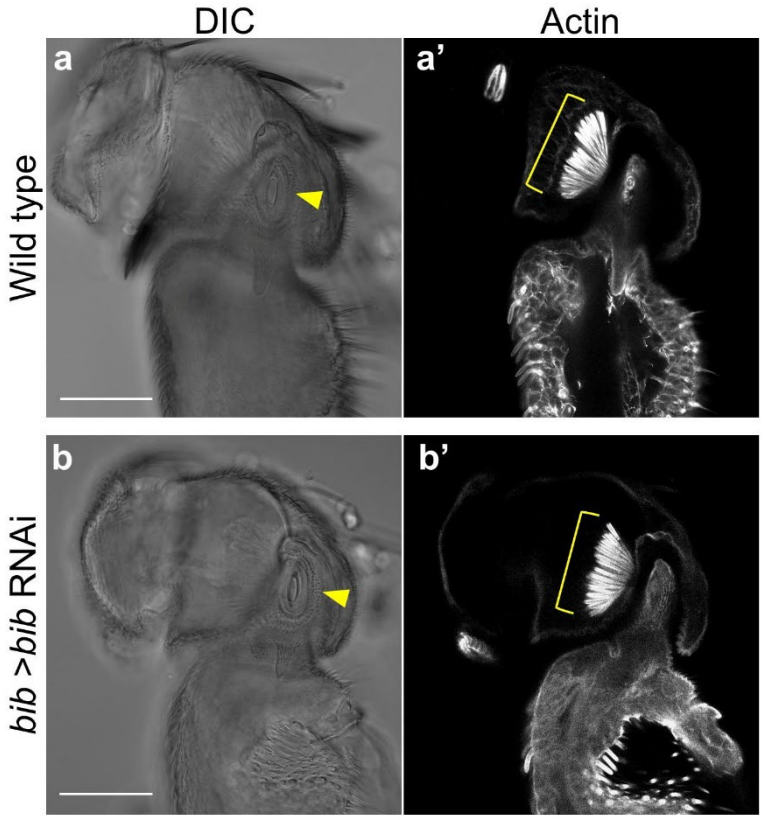


Fig. S2 Lack of visible effect of *bib* knockdown on the a2-3 joint and JO. Mature antennae of a wild-type pharate adult (pupa with red eyes and black wings) (a, a') and a *bib* RNAi pupa at 72 hours APF (b, b') viewed along the lateral-medial axis. Cuticle morphology is visualized in differential interference contrast (DIC) images (a, b). The ring-like morphology of the a2-a3 joint (see Fig. 1n) is clearly observed in both wild-type and *bib* RNAi (arrowheads). JO morphology is revealed by actin staining (a', b'). Scolopidia converge on the a2-a3 joint in both wild-type and *bib* RNAi (brackets). All images in this

figure are horizontally flipped. Scale bars: 50 μm.

Table S1 Genotypes of flies used in the figures.

| **Figure** | **Genotype** |
|---|---|
| Fig. 1a-h, 1j-n, 2c | *y*$^{1}$ *w*$^{67c23}$; UAS-mCD8::GFP.L$^{LL5}$ *Dll*$^{md23}$, UAS-mCD8::GFP.L$^{2}$/ CyO |
| Fig. 1i, 3g, 5, S1f | *w**; *Dll*$^{md23}$, UAS-mCD8.ChRFP$^{2}$/ *nompA.GFP*$^{5-3}$ |
| Fig. 2a-b, 3b-c', 3e-f, S1a-b, S1d-e | *w**; *nompA.GFP*$^{5-3}$/ 10XUAS-IVS-mCD8::RFP$^{attP40}$; *prosV1* / + |
| Fig. 3d, S1c-c', 6 | *w**; *nompA.GFP*$^{5-3}$/ *bib*$^{NP5149}$ UAS-mCD8.mRFP.LG$^{18a}$ |
| Fig. 7a | *w**; *fng*$^{NP6586}$/ 20XUAS-IVS-mCD8::GFP$^{attP2}$ |
| Fig. 7b | *w**; *neur*$^{NP1357}$/ 20XUAS-IVS-mCD8::GFP$^{attP2}$ |
| Fig. S2a | Canton-S |
| Fig. S2b | *y**; *bib*$^{NP5149}$ UAS-mCD8.mRFP.LG$^{18a}$/ +; UAS-*bib* RNAi$^{JF02771}$/ + |